THERMALLY INDUCED ELECTROCONVECTION

by

J. Wong and J. R. Melcher

CSR-TR-69-3 February 7, 1969

CENTER FOR SPACE RESEARCH
MASSACHUSETTS INSTITUTE OF TECHNOLOGY

THERMALLY INDUCED ELECTROCONVECTION

by

J. Wong and J. R. Melcher

CSR-TR-69-3 February 7, 1969

THERMALLY INDUCED ELECTROCONVECTION

by

J. Wong and J. R. Melcher

Abstract

The combined effects of a thermal gradient and a dc electric field upon a poorly conducting fluid are used to induce steady convection. A natural, vertically-directed temperature gradient is used to establish an electrical conductivity gradient over the rectangular cross-section of a liquid-filled channel. Then a static potential, which varies either linearly or periodically along the channel, is imposed on electrodes that form the channel top. A similar potential, spatially shifted in the longitudinal (horizontal) direction, is applied at the bottom of the channel. These electrodes make physical and electrical contact with the fluid, which typically has a mean electrical conductivity of 10^{-10} mhos/m. Because of the conductivity gradient, the vertical component of the resulting electric field induces free charges in the bulk, and these charges are then pulled in the horizontal direction by the longitudinal component of the electric field. An analytical model is used to predict the distribution of potential, electric stress, and velocity.

It is assumed that effects of convection on the charge distribution can be ignored (electric Reynolds number small). An experiment is described in which the periodic potential distribution is closed on itself in a reëntrant channel to achieve fully developed flow. Experiment and theory compare favorably with discrepancies attributable largely to finite electric Reynolds number effects.

I. Introduction

A. Physical Phenomenon

Natural convection, as it obtains in fluids subject to the combination of thermal gradients and gravitational forces, is the basis for the transport of heat and mass[1] in practical situations that range from the cooling of utilities transformers[2] to atmospheric circulations[3]. Thus it is the simple basic mechanism of the buoyancy force induced by a thermal gradient that forms the theme for an area of fluid mechanics[4].

There is a similar class of electrohydrodynamic flows obtained by applying both an electric field intensity $\overline{E}$ and a temperature gradient ∇T to a fluid of slight electrical conductivity. In these cases, the buoyancy force responsible for natural convection is augmented or even replaced by an electro-thermally induced force density. The electric force density, which is well known[5,6], is the consequence of a charge accumulation due to an electrical current component having the same direction as the thermally induced electrical conductivity gradient. That is, the natural electrical conductivity, σ, is temperature-dependent in most liquids generally regarded as electrical insulators ($\sigma < 10^{-8}$ mhos/m). Thus, if there is a local gradient in temperature induced by a thermal flux, there is an accompanying gradient in σ, and a space charge density, q, given by

$$q = \nabla\cdot\varepsilon\overline{E} = \nabla\cdot\left(\frac{\varepsilon\overline{J}}{\sigma}\right) = -\left(\frac{\varepsilon\overline{J}}{\sigma^2}\right)\cdot\nabla\sigma \qquad (1)$$

where it is assumed that thermally induced variations in the permittivity are negligible in effect, that steady conditions prevail, and that the conduction current density $J = \sigma\overline{E}$ dominates the convection current $q\overline{v}$ (caused by the fluid velocity $\overline{v}$) so that $\nabla\cdot\overline{J} = 0$.

As an example, suppose that the electric field intensity and conductivity gradient at a given point in the fluid were as shown in Fig. 1. Then, the charge induced would be negative, and the electrical force $q\overline{E}$ would be in a direction opposite to $\overline{E}$. As with natural convection, motions in the direction of the thermal gradient tend to destroy both the thermal and conductivity gradients. These motions are therefore at a rate limited by the longest relaxation or diffusion time for maintaining the driving gradients. Depending on the fluid properties and the particulars of the configuration, the flow can be limited by a thermal time constant for maintaining the temperature gradient in the face of the convection, or by an electrical relaxation time required for the accumulation of space charge.

In contrast, convection perpendicular to the thermal and conductivity gradients does not tend to destroy these gradients, and can therefore proceed at a faster rate. For the example of Fig. 1, such motions would be in the x (longitudinal) direction. The transverse field component E_y then serves the purpose of creating the space charge, but also produces a force density that must be balanced by hydrostatic pressure.

Two cases are developed in the following sections. In the first, an electric field with both transverse and longitudinal components is produced in the volume of a channel flow by imposing potential distributions on the channel top and bottom that vary linearly with longitudinal distance. The points of zero potential are displaced longitudinally, so that both of the required components of $\overline{E}$ are present. Of course, there is only a limited distance over which the potentials can be practically made to vary linearly. A second configuration obviates this difficulty by using spatially periodic potential distributions, with that on the bottom shifted in phase with res-

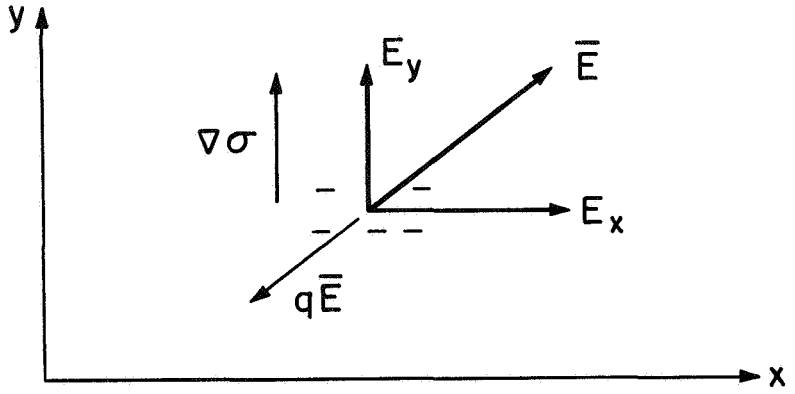

Fig. 1 The component of electric field intensity E_y in the direction of the conductivity gradient $\nabla\sigma$ leads to the local accumulation of space charge. The electrical force is in the direction of $\bar{E}$, hence has a component in the x direction.

pect to that on the top. The fact that steady convection results can be traced directly to the important fact that the space charge is induced by the same field that is responsible for producing the force. Thus a reversal of the field polarity also reverses the sign of the charge [Eq. (1)], and hence leaves the sign of the force unchanged.

B. Background

A study has illustrated the fact that a traveling wave of potential can be used to induce convection perpendicular to the electrical conductivity gradient produced by a temperature gradient.[7] Although there are many similarities between that interaction and the second case described here, there are also essential differences. Here, the applied fields are static. This means that the potential distributions must be imposed with electrodes that make electrical contact with the fluid. Otherwise, there would be no conduction current from the external sources of potential to the fluid, and the fluid would polarize in such a way as to exclude the electric field from the bulk. In the traveling wave "induction interactions", the charges are induced at one point in the fluid bulk at the expense of charges at another point; there is no requirement for electrical contact with the fluid.

There is the important question of whether or not hydrostatic pressure can be used to equilibrate the transverse force produced by the component E_y used to induce the space charge. If it is assumed that the temperature profile is natural, than gravitational buoyancy forces tend to stabilize the profile. However, there remains the possibility of instability produced by the transverse electrical forces. For such an instability, there is a threshold which, for no longitudinal $\bar{E}$, has been predicted and measured[8,9]. In the following developments, it is assumed that the threshold for instability is

not exceeded, and in the periodic potential case where the transverse force is not constant, that secondary convection from the transverse forces is not of significance.

II. Spatially Linear Potential

A. Configuration

A cross-sectional view of the plane flow configuration is shown in Fig. 2. Electrodes at $y = \pm\ell$ are constrained in potential ϕ such that

$$\phi(x,\ell) = V_m(x-x_o)/\ell \; ; \quad \phi(x,-\ell) = V_m\, x/\ell \tag{2}$$

These distributions are sketched in Fig. 2, together with the lines of constant potential and electric field intensity found in Sec. IIB. The position of zero potential on the upper electrodes is shifted with respect to that on the lower electrodes by the distance x_o. Note from Eq. (1) that, if the conductivity increases with depth, the transverse component of $\overline{E}$ gives rise to a negative bulk charge, and this conspires with the longitudinal component of $\overline{E}$, which is negative, to produce an electrical force density tending to propel the fluid in the positive x direction.

Because the temperature variation only serves to create the conductivity gradient, the thermal aspects of the problem are a secondary consideration. In fact, any stratification mechanism that leads to the electrical conductivity profile

$$\sigma = \sigma_o + \sigma_1 y/\ell \tag{3}$$

σ_o and σ_1 constants, would be described by the analytical model now derived.

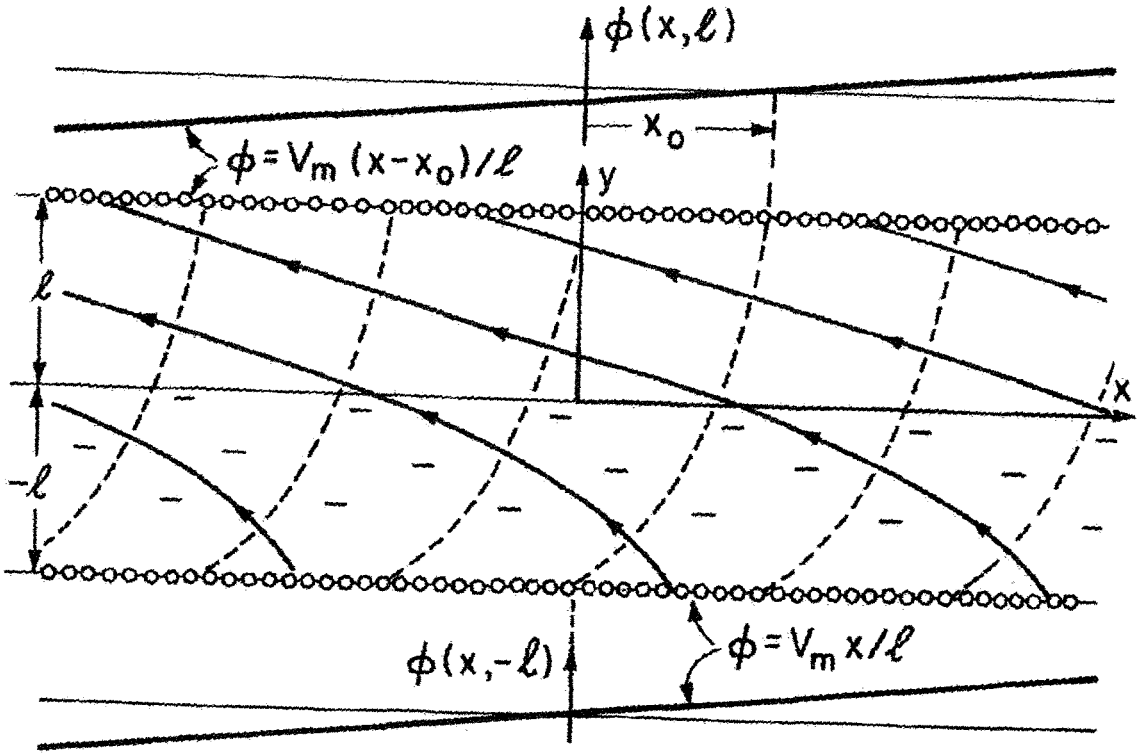

Fig. 2 Cross-sectional view of plane flow configuration with linear potential distributions imposed on the channel bottom and top. Lines of constant potential and electric field intensity are shown, as well as the induced space charge density. For the case shown, the fluid is pumped to the right.

B. Potential Distribution

Under steady-state conditions, with the convection current ignored, conservation of charge requires that

$$\sigma\nabla^2\phi + \nabla\sigma\cdot\nabla\phi = 0 \tag{4}$$

where $\overline{E} = -\nabla\phi$. The essentials of the interaction are retained if the first coefficient in Eq. (4) is approximated by the mean conductivity, σ_o. Then, Eq. (4) becomes

$$\frac{\partial^2\phi}{\partial y^2} + \alpha\frac{\partial\phi}{\partial y} + \frac{\partial^2\phi}{\partial x^2} = 0 \tag{5}$$

where $\alpha = \sigma_1/\sigma_o\ell$.

The solution to Eq. (5) which satisfies boundary conditions (2) is

$$\phi = V_m\left[\frac{x}{\ell} + \frac{x_o}{\ell}\left(\frac{e^{-\alpha y} - e^{\alpha\ell}}{2\sinh\alpha\ell}\right)\right] \tag{6}$$

This potential distribution, and the implied electric field intensity, is illustrated in Fig. 2.

C. Electrical Stress and Velocity Profiles

For plane Couette flow, $\overline{v} = v_x(y)\overline{i}_x$ and there are no contributions to the longitudinal force balance from pressure or inertia. Thus, the x-component of the equation of motion equilibrates the electrical and viscous force densities

$$\frac{\partial}{\partial x}T_{xx} + \frac{\partial}{\partial y}T_{xy} = -\frac{\partial}{\partial y}\left(\mu\frac{\partial v_x}{\partial y}\right) \tag{7}$$

where $T_{ij} = \varepsilon E_i E_j - \frac{1}{2}\delta_{ij}\varepsilon E_k E_k$ and μ is the viscosity. The Maxwell stress component T_{xx} is independent of x, so that Eq. (7) can be integrated twice on y to give

$$v_x = -\frac{1}{\mu}\int_{-\ell}^{y} T_{xy}\, dy + \frac{(y+\ell)}{2\mu\ell}\int_{-\ell}^{\ell} T_{xy} dy \tag{8}$$

Note that the electrodes at $y = \pm\ell$ contact the fluid physically, so that Eq. (8) must satisfy the conditions $v_x(\ell) = v_x(-\ell) = 0$.

Although it is straightforward to take account of the variation of viscosity with depth, the complexity of the predictions obscure the physics of interest, and μ has been taken as a constant (the average) in the second integration of Eq. (7). From Eq. (6), it follows that the electric shear stress is

$$T_{xy} = \varepsilon E_x E_y = -\alpha\varepsilon\left(\frac{V_m}{\ell}\right)^2 \frac{x_o\, e^{-\alpha y}}{2 \sinh \alpha\ell} \tag{9}$$

and hence the required velocity profile follows from Eqs. (8) and (9) as

$$v_x(y) = -\frac{\varepsilon x_o}{2\mu}\left(\frac{V_m}{\ell}\right)^2 \left[\frac{y}{\ell} + \frac{(e^{-\alpha y} - \cosh \alpha\ell)}{\sinh \alpha\ell}\right] \tag{10}$$

For the case with α positive, so that the more insulating fluid is at the bottom of the channel, the electrical force density $\partial T_{xy}/\partial y$ and the shear stress are seen from Eq. (9) to be the largest at the bottom. Thus, the peak in velocity as given by Eq. (10) falls somewhat below the channel midplane at $y = -\ell n(\sinh \alpha\ell/\alpha\ell)/\alpha$.

The nature of thermally induced electroconvection in static electric fields is illustrated by Eq. (10). The direction of flow is determined by the spatial relationship of the imposed potentials (x_o) and not by the sign of the imposed potential V_m.

Note that the transverse force density implied by Eq. (6) is independent of the longitudinal position x, and is therefore balanced by the hydrostatic pressure. However, it is this force component that plays a part in instability.

III. Spatially Periodic Potential

A. Configuration

It is clear from the concluding remarks to Sec. IIC that the longitudinal force density in the linear potential configuration of Fig. 2 remains positive if the potential distributions are decreasing, rather than increasing, functions of x. The shift x_o determines the direction of flow.

A natural evolution of the linear potential distribution case, to obtain a channel of arbitrary length, is sketched in Fig. 3a. The potential distributions are now spatially periodic, with a phase difference of $x = \theta/k$. Over the ranges of x where the slopes of the imposed potential distributions are of the same sign, the channel configuration is essentially the same as for the linear distribution. Of course, there are now spatial variations in both components of the force density. The flow response of the fluid to the electrical stress averaged over one wavelength is computed.

B. Potential Distribution

The potential distributions are approximated by the first Fourier components, so that boundary conditions are

$$\phi(x,\ell) = \mathrm{Re}\ V_o\, e^{-j(kx-\theta)}; \quad \phi(x,-\ell) = \mathrm{Re}V_o\, e^{-jkx} \tag{11}$$

To match these conditions, solutions are assumed of the form $\phi = \mathrm{Re}\ \hat{\phi}(y)\exp(-jkx)$, where it then follows from Eq. (5) that

$$D^2\hat{\phi} + \alpha D\hat{\phi} - k^2\hat{\phi} = 0 \quad ; D(\ ) \equiv d(\ )/dy \tag{12}$$

It follows that $\phi \propto \exp(py)$, where

$$p = -\frac{\alpha}{2} \pm \beta \ ; \quad \beta = [(\alpha/2)^2 + k^2]^{\frac{1}{2}} \tag{13}$$

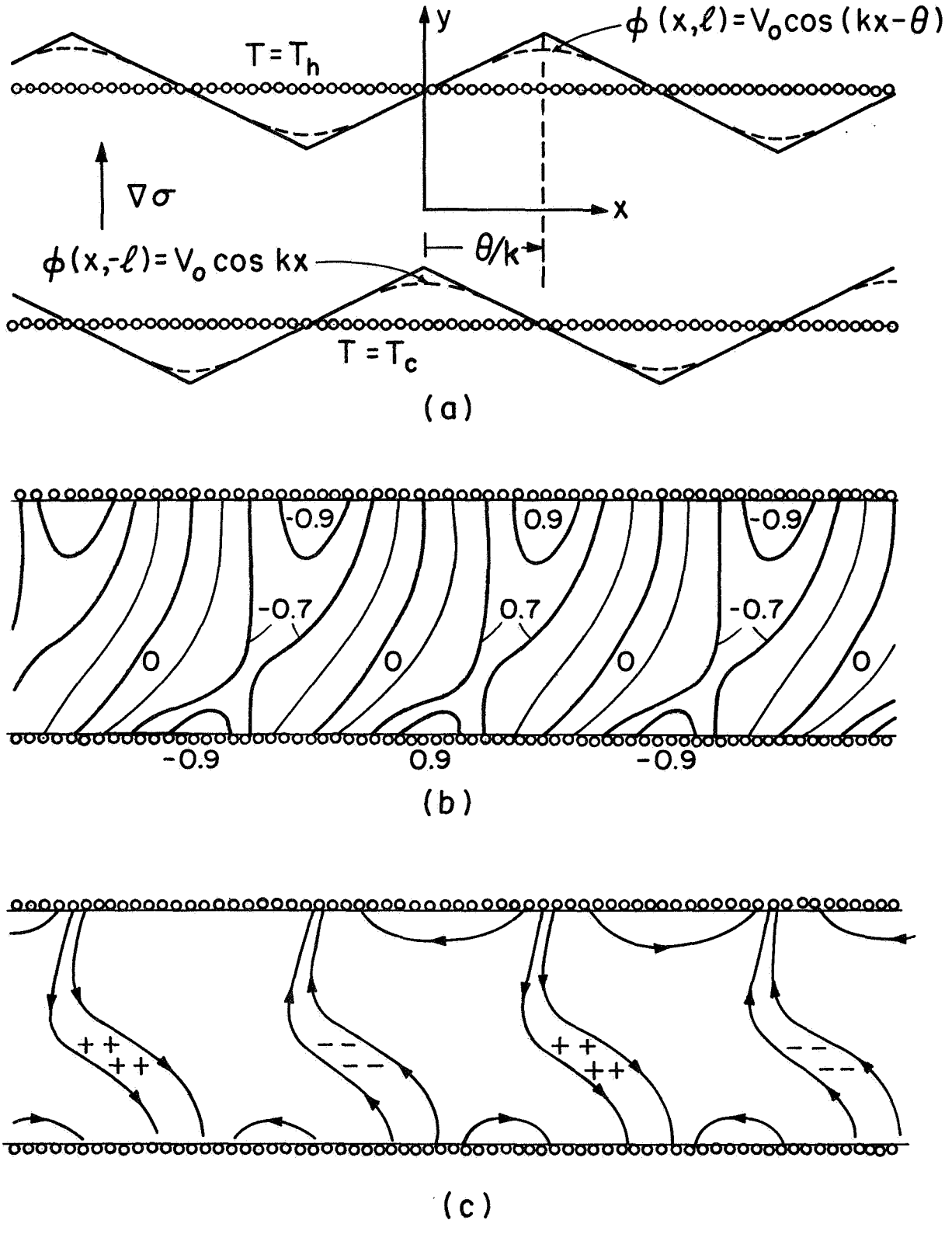

Fig. 3 Cross-sectional view of flow configuration with spatially periodic distribution of imposed potential. (a) Electrode potential distributions. (b) Potential distribution in fluid bulk ($\alpha >> k$). (c) Lines of electric field intensity and induced space charge, showing regions that contribute to a force density in the x direction.

A linear combination of solutions, Eq. (13), that satisfies the boundary conditions (11) is

$$\hat{\phi} = \frac{V_o e^{-\frac{\alpha y}{2}}}{\sinh 2\beta\ell}\left[e^{j\theta + \frac{\alpha}{2}\ell} \sinh \beta(\ell+y) + e^{-\frac{\alpha}{2}\ell} \sinh\beta\,(\ell-y)\right] \qquad (14)$$

A sketch of this potential distribution with $\theta = \pi/2$ used for the case $\alpha >> k$ is shown in Fig. 3b, and Fig. 3c illustrates the implied lines of electric field intensity and space charge. In regions where the potential slopes on the channel top and bottom are of like sign, the potential and field distributions have the character of those for the linear distribution. In the intervening regions, the fields tend to produce undesirable forces in the transverse and longitudinal directions.

C. Electrical Stress and Velocity Distributions

Under the assumption of plane Couette flow, Eq. (7) is again appropriate. It is assumed that the fluid responds to the electrical force averaged over one wavelength. Thus, the first term in Eq. (7) makes no contribution, and it is the spatially averaged value of shear stress $\langle T_{xy} \rangle$ that is required in the second term. To compute $\langle T_{xy} \rangle = \langle \varepsilon E_x E_y \rangle$, use is made of the identity $\langle \mathrm{Re}\,\hat{A}\,e^{-jkx}\ \mathrm{Re}\,\hat{B}\,e^{-jkx} \rangle = \frac{1}{2}\,\mathrm{Re}\,\hat{A}^*\hat{B}$, and Eq. (14), to write

$$\langle T_{xy} \rangle = \frac{1}{2}\,\mathrm{Re}(jk\varepsilon\hat{\phi}^* D\hat{\phi}) = -\varepsilon V_o^2 \beta k\, e^{-\alpha y} \sin\theta/2 \sinh 2\beta\ell \qquad (15)$$

With this result, Eq. (8) is integrated to obtain the velocity profile

$$v_x = \varepsilon k V_o^2\, \beta \sin\theta\, [\cosh\alpha\ell - e^{-\alpha y} - (\tfrac{y}{\ell})\sinh\alpha\ell]/2\mu\alpha \sinh 2\beta\ell \qquad (16)$$

The same attributes are apparent here as for the linear case, Eq. (10), except that the phase shift now gives a largest positive velocity as $\theta = \pi/2$; the phase shift illustrated in Fig. 3 and used in the experiment of Sec. IV. Note that

the peak velocity is at the same position as for the linear case.

IV. Experiments

An apparatus for studying the electroconvective pumping is shown in Fig. 4. Plexiglas channel walls support brass rods that both impose the required periodic longitudinal variation in potential and constrain the longitudinal velocity of the adjacent fluid to be essentially zero. The liquid extends above the upper electrodes, where, at the beginning of a test, the temperature is raised to T_h. Because the time constant for conduction of heat to the fluid at the bottom is long compared with the time required for a test run, no heat sink is required to maintain the temperature T_c in the region of fluid below the bottom electrodes.

Experiments, conducted by using a linear potential distribution imposed essentially as described in Sec. II, result in velocities that are in reasonable agreement with the prediction of Eq. (10)[10]. For these tests, the electrodes are placed only in a section of the reëntrant channel which has a length of 15 cm. As a result, the conditions of fully developed flow in the interaction region are not met; moreover, the pressure drop due to the return circulation of the fluid is not accounted for by the theory.

The imposition of an integral number of wavelengths of a periodic potential on electrodes that extend over the circumferential length of the channel makesit possible to maintain control over the flow conditions. The circumstances predicated in Sec. III. are then more closely approximated. Hence, only data found for the spatially periodic case are presented here.

Physical parameters for the experiments are summarized in Table I and Fig. 4. The velocity, which for the experimental conditions has its peak value essentially at the channel center, is measured by injecting a small amount of the working fluid (corn oil) with dye added. This is done in such a way that the electrical and thermal profiles are not altered appreciably. In any case,

Fig. 4 Reëntrant channel for studying flow induced by spatially periodic potentials, showing side and end views of channel. The mean length of the channel is 2.43 m, so that there are nine wavelengths of potential imposed on the electrodes. The channel is shown without the voltage divider and connecting wiring for electrodes.

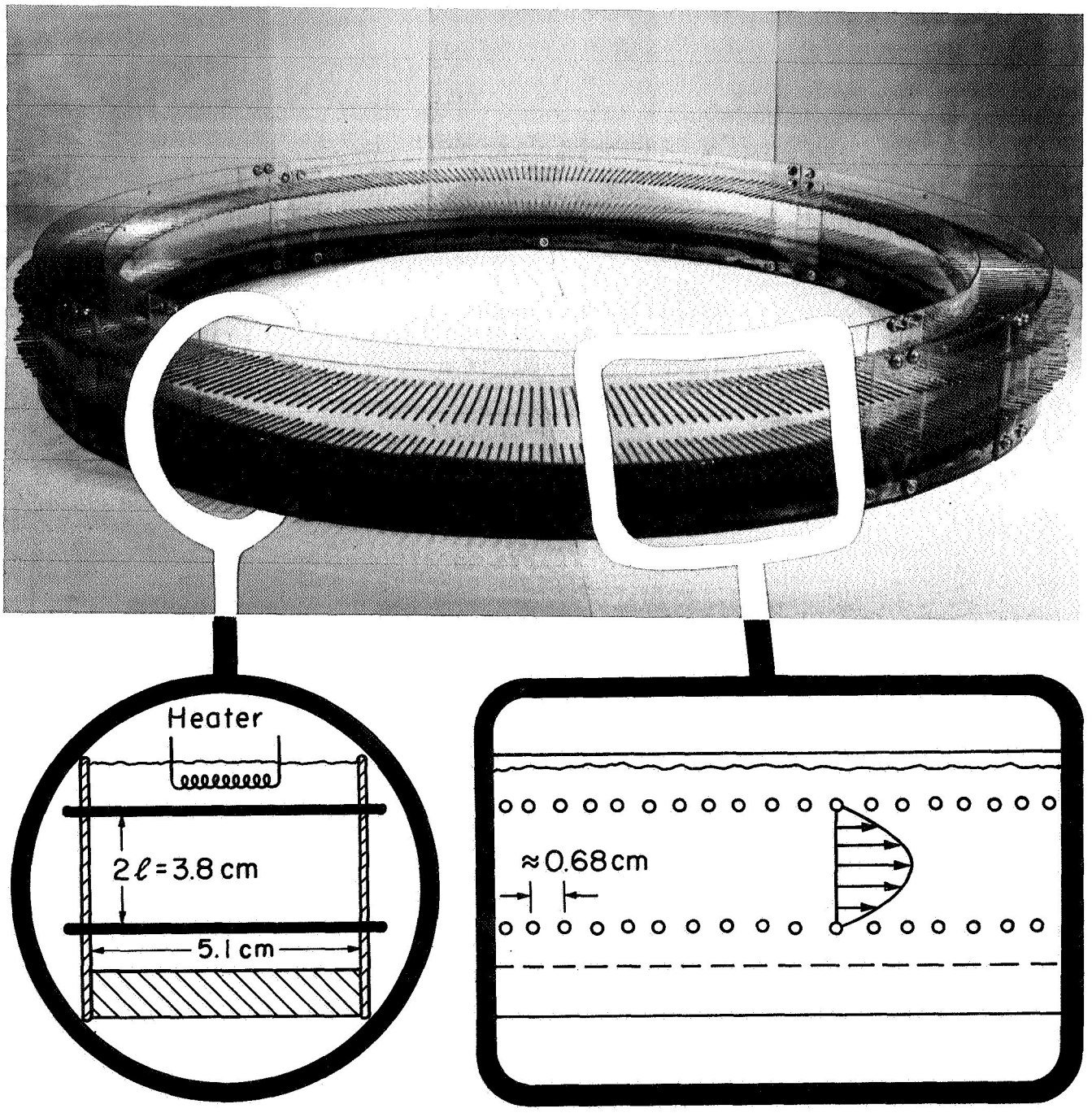

the use of the dye marker and a stop watch for velocity measurements involves only a wavelength or so of the nine wavelengths. Because each wavelength is in flow series with the next, local disturbances tend to be smoothed out.

All measurements are taken with the phase shift for maximum velocity; $\theta = \pi/2$. The voltage V_p is the peak potential of the sawtooth potential distribution sketched in Fig. 3a and imposed on the channel electrodes with voltage dividers. In the theoretical model, the first Fourier component of this distribution is used, with a peak potential $V_o = 0.85\ V_p$. Then, according to Eq. (16), a normalized velocity at the channel center is

$$v_s = v_x(0)\ \frac{\alpha \sinh 2\beta\ell}{2\beta(\cosh \alpha\ell - 1)} = \frac{\varepsilon k}{4\mu}\ 0.72\ V_o^2 \qquad (17)$$

Note that v_s is the velocity normalized so that experiments which differ in conductivity profile, but have the same mean viscosity, should have the same dependence on V_p.

Experimental measurements, together with the prediction provided by Eq. (17) are shown in Fig. 5. It must be recognized that variations in the viscosity across the channel have been ignored, and that the electrical conductivity is not an entirely stable fluid parameter, even for corn oil, a fluid chosen for its relative stability. Thus, the quantitative disagreement between the theoretical model and measurements represented by Fig. 5 is consistent with uncertainties in the physical parameters used in Eq. (17).

V. Concluding Remarks

The intention of this work is to demonstrate quantitatively, in as simple a manner possible, the class of electrohydrodynamic flows found as slightly conducting fluids are simultaneously stressed by constant electric

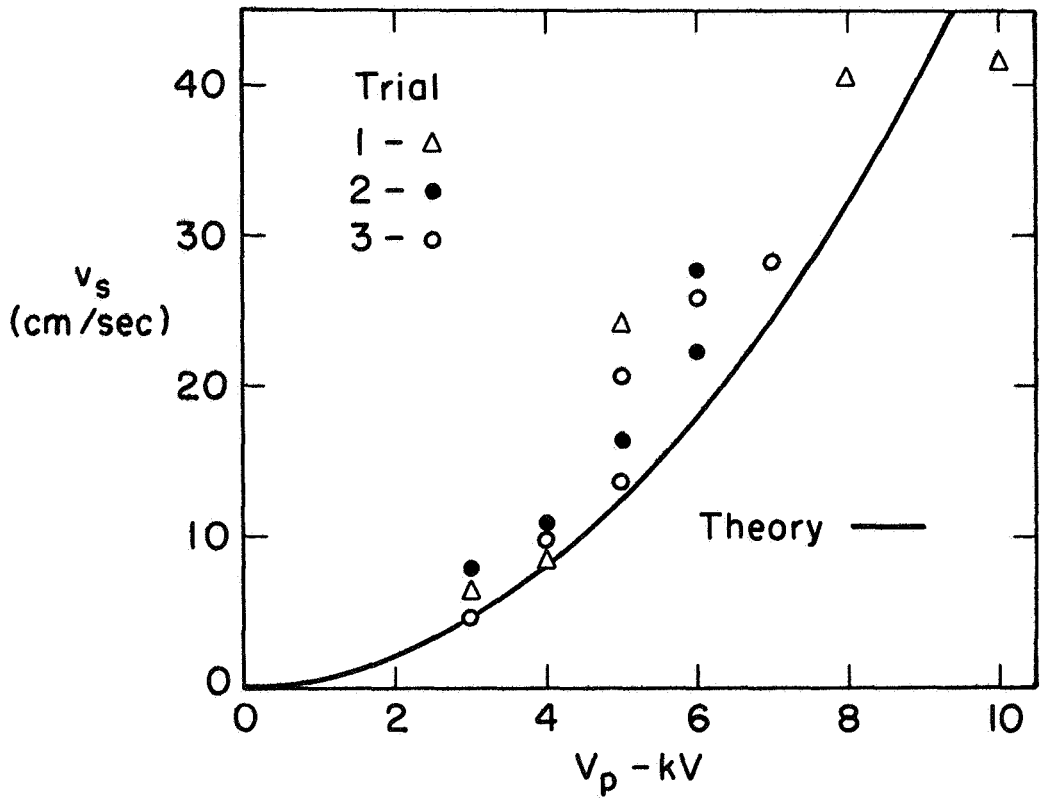

Fig. 5 Mean velocity at channel center for three trials. v_s is defined in terms of $v_x(0)$ by Eq. (17). For trials nos. 1 and 3, the actual velocity in cm/sec. is 0.099 v_s, while for trial No. 2 it is 0.13 v_s; V_p is the peak voltage of the sawtooth waveform.

fields and a thermal flux. As with natural convection, these flows become considerably more complicated to describe if there is a coupling between the convection and either the thermal or the electrical gradients that drive the convection. For the flows transverse to the thermal gradient discussed here, the thermal gradient is left undisturbed by the convection. However, in the case of the periodic potential distribution, the electrical relaxation process does enter as a limitation on the flow rate. The electric Reynolds number is a measure of the error committed in Eq. (4) by ignoring the electric convection current density, $\overline{v}q$. Note that, with the constant coefficient approximation, the first term in Eq. (4) is $\sigma_o q/\varepsilon$, and it is clear that the convection current contribution can be ignored, if

$$|\sigma_o q/\varepsilon| \gg |\overline{v}\cdot\nabla q| \tag{18}$$

This inequality requires that the electric Reynolds number $R_e = \varepsilon v_x k/\sigma$ be small compared with unity. The experiments reported in Sec. IV satisfy this condition, with R_e at most 0.25.

It is clear that further studies are called for to explore the consequences of finite thermal diffusion and electrical relaxation processes. These processes, along with instabilities connected with both the static equilibrium and the shear flow, are the primary limitations on the breadth of practical applications for this class of flows.

Acknowledgments:

The authors greatly appreciate the help of Miss Stephanie Wong, Mr. Harold Atlas, and Mr. E. Paul Warren. This work is supported by NASA Grant No. NGL-22-009-014.

References

1. Rohsenow, W. M., and Choi, H. Y., Heat, Mass and Momentum Transfer, Prentice-Hall,Inc., Englewood Cliffs, N. J. (1961), p. 88.

2. Blume, L. F., et al, Transformer Engineering, John Wiley & Sons, Inc. New York, N. Y. (1951), 2nd. Ed., p. 300.

3. Greenspan, H. P., The Theory of Rotating Fluids, Cambridge University Press, Cambridge, England (1968), p. 293.

4. Eckert, E. R. G., and Gross, J. F., Introduction to Heat and Mass Transfer, McGraw-Hill Book Company, Inc., New York, N.Y. (1963), pp. 186-196.

5. Stratton, A. S., Electromagnetic Theory, McGraw-Hill Book Company, Inc. New York, N. Y. (1941), p. 222.

6. Woodson, H. H., and Melcher, J. R., Electromechanical Dynamics, Part II: Fields, Forces and Motion, John Wiley & Sons., Inc., New York, N. Y., p. 378.

7. Melcher, J. R., and Firebaugh, M. S., Phys. Fluids, 10, p. 1178 (1967)

8. Turnbull, R. J., Phys. Fluids, to be published

9. Turnbull, R. J., Phys. Fluids, to be published

10. Wong, J., "Thermally Induced Electroconvection in DC Fields", M.S. Thesis, Dept. of Electrical Engineering, Massachusetts Institute of Technology, Cambridge, Mass., (1968).

Trial	T_h (°C)	T_c (°C)	σ_o (mho/m)	σ_1 (mho/m)
1	53	37	1.06×10^{-10}	0.24×10^{-10}
2	60	38	1.21×10^{-10}	0.37×10^{-10}
3	55	37	1.08×10^{-10}	0.25×10^{-10}
$\varepsilon = 3.1\ \varepsilon_o$ $\quad \lambda = 2\pi/k = 0.27$ m				
$\mu = 2.25 \times 10^{-2}$ kg/m-sec. $\quad \ell = 1.9$ cm				

Table I. Physical parameters and apparatus dimensions for trial runs of Fig. 5.